Tellus (2007), 59A, 292–308
Printed in Singapore. All rights reserved

TELLUS

Validating and understanding the ENSO simulation in two coupled climate models

By VASUBANDHU MISRA*, LARRY MARX, JAMES L. KINTER III, BEN P. KIRTMAN, ZHICHANG GUO, DUGHONG MIN, MIKE FENNESSY, PAUL A. DIRMEYER, RAMESHAN KALLUMMAL and DAVID M. STRAUS, *Center for Ocean-Land-Atmosphere Studies, Institute of Global Environment and Society, Inc. 4041 Powder Mill Road, Suite 302, Calverton, MD 20705, USA*

(Manuscript received 29 July 2006; in final form 19 January 2007)

ABSTRACT

A newly developed Atmospheric General Circulation Model (AGCM) at T62 spectral truncation with 28 terrain-following ($\sigma = \frac{p}{p_s}$) levels coupled to the Modular Ocean Model version 3.0 (MOM3.0) is evaluated for its simulation of El Niño and the Southern Oscillation (ENSO). It is also compared with an older version of the AGCM coupled to the same ocean model. A dozen features of ENSO are validated. These characteristics of ENSO highlight its influence on global climate at seasonal to interannual scales.

The major improvements of the ENSO simulation from this new coupled climate model are the seasonal phase locking of the ENSO variability to a realistic annual cycle of the eastern equatorial Pacific Ocean, the duration of the ENSO events and its evolution that is comparable to the ocean data assimilation. The two apparent drawbacks of this new model are its relatively weak ENSO variability and the presence of erroneous split ITCZ.

The improvement of the ENSO simulation in the new coupled model is attributed to realistic thermocline variability and wind stress simulation.

1. Introduction

El Niño and the Southern Oscillation (ENSO) variability is one of the largest sources of interannual variability driven by coupled climate processes (Philander, 1983, 1990) that has ramifications on the global climate (Rasmusson and Carpenter, 1982; Ropelewski and Halpert, 1987; Trenberth et al., 1998; Goddard and Dilley, 2005). Warm (cold) ENSO episodes are characterized by increased (decreased) SST in the central and the eastern equatorial Pacific Ocean with a broad-band periodicity of 2 to 7 yr. This variation in SST has concomitant changes in the surface wind stress, sea level pressure and ocean heat content as well as the teleconnection patterns of precipitation, surface temperature, and tropospheric temperature that are manifestations of the complex interactions of the coupled ocean–land–atmosphere dynamical system. The variations in the tropical Pacific are primarily due to coupled ocean–atmosphere modes (Philander, 1983; Suarez and Schopf, 1988; Jin, 1997), while the tropical and extratropical teleconnections occur primarily through atmospheric bridges (Lau and Nath, 1996; Alexander et al., 2002).

*Corresponding author.
e-mail: misra@cola.iges.org
DOI: 10.1111/j.1600-0870.2007.00231.x

In this study, we first validate the simulation of ENSO in two different versions of a CGCM. The CGCM used in this study has as its atmospheric component the Center for Ocean-Land-Atmosphere Studies (COLA) Atmospheric General Circulation Model (AGCM) Version2.2 (V2.2) and the recently updated COLA AGCM Version3.2 (V3.2). The AGCMs incorporate a model of the land surface as described in the following section. The ocean model is the Modular Ocean Model Version 3.0 (MOM3; Pacanowski and Griffies, 1998). The realism of ENSO simulations has been evaluated in several studies (Neelin et al., 1992; Mechoso et al., 1995; Latif et al., 2001; van Oldenborgh et al., 2005; Capotondi et al., 2006; Guilyiardi, 2006; Joseph and Nigam, 2006; Rao and Sperber, 2006).

In this paper, we have highlighted 12 features related to ENSO suitable for verifying the credibility of a global coupled model simulation. We argue that these features compose a necessary but not sufficient condition for a successful simulation of ENSO. In addition, we restrict the analysis to these 12 features due to the constraints of the available observations and our limited understanding of the phenomenon. The 12 features are as following:

(1) Mean upper ocean and precipitation errors in the tropics.
(2) Mean annual cycle of the Equatorial Pacific SST and wind stress.
(3) Temporal Variability of the Niño3 SST.

(4) Seasonal phase locking of the Niño3 SST variability.
(5) ENSO related SST and upper Ocean variability.
(6) Duration of ENSO events.
(7) Evolution of SST in the equatorial Pacific.
(8) Evolution of the subsurface ocean temperatures in the equatorial Pacific.
(9) Relationship of the Niño3 SST variability with the tropical Oceans.
(10) Relationship between Niño3 SST and wind stress.
(11) Relationship between Niño3 SST and precipitation.
(12) Mid-latitude atmospheric response to ENSO.

Despite the many intercomparison studies of coupled models, and mechanistic and process studies relating to ENSO, there are considerable gaps in our understanding of the phenomenon that is largely reflected in the relatively poor prediction and simulation skill of state of the art CGCMs. Most current coupled models have an erroneously split intertropical convergence zone (ITCZ), cold bias in the equatorial eastern Pacific, a warm bias off the South American and the South African coasts, a tropical thermocline that is too diffuse, insufficient upwelling along the eastern boundaries of continents, interannual variability that extends too far to the west and is narrow and weak along the equator. These deficiencies have been documented in a workshop on tropical biases in coupled models (ftp://grads.iges.org/pub/schneider/CTBW05/Previous_mtg/Ping_CLIVAR_summary.pdf;ftp://grads.iges.org/pub/schneider/CTBW05/Previous_mtg/EPIC_tropbias_Bretherton.2003.pdf). In addition, many models exhibit a strong biennial cycle in the SST variability over the eastern Pacific that is unsupported by observations. Some of these issues persist in the two coupled climate models used in this study as well. It should however be noted that these deficiencies act as a limiting barrier on the predictability of ENSO in the current state-of-the art coupled climate models.

The details of the coupled model used in this study are outlined in the following section followed by a description of the design of experiments. The results are presented in Section 4. In Section 5, we discuss the results to understand the differences in the ENSO simulation between the two coupled models followed by concluding remarks in Section 6.

2. Model description

2.1. Atmospheric general circulation model

A new AGCM has been recently developed at COLA (COLA AGCM V3.2; hereafter V3.2). The previous version of the COLA AGCM (V2.2) which formed the basis for the current version of the AGCM has been extensively used for coupled climate modelling studies in the past (Kirtman and Shukla, 2002; Kirtman et al., 2002; Schneider, 2002; Kirtman, 2003). However, it should be noted that V2.2 had some serious flaws in its mean climate as well as in its ENSO simulation with annual mean errors of SST in excess of 5° in the tropical Pacific.

V3.2 has a revised subgrid scale physical parametrizations package compared to V2.2 (Table 1). An important aspect of V3.2 is that the atmospheric component has been tuned to produce a reasonable mean climate that balances the energy at the top of the atmosphere and at the surface to within a couple of W m^{-2} when coupled to the ocean model (MOM3). Many climate modelling centres develop component models independent of each other before finally coupling them. The latter approach does not account for the biases that arise as a result of errors in coupling the components of the climate system and the nonlinear coupled error growths arising in the dependent variables of the component models. Furthermore, by forcing (tuning) the climate of the component models to behave reasonably relative to observations without taking into account coupled processes can give rise to additional biases in the coupled climate system (Wu et al., 2006).

The tuning in V3.2 involved modulating the vertical profile of diabatic heating through the adjustment of the fractional amount of large-scale and convective precipitation that is evaporated into the environment, the critical relative humidity to diagnose saturation cloud fraction and the order of a spatial filter used to smooth the inversion clouds (which is required as a result of the spectral truncation) that significantly affected the bias over the

Table 1. The outline of the physics package in the AGCM used in the study (V3.2) and its comparison with the previous version (V2.2)

Process	V3.2	V2.2
Deep convection	Relaxed Arakawa Schubert scheme (Bacmeister et al., 2000)	Relaxed Arakawa Schubert scheme (Moorthi and Suarez, 1992)
Longwave radiation	Collins et al. (2002)	Harshvardhan et al. (1987)
Boundary layer	non-local (Hong and Pan, 1996)	level 2.0 closure (Mellor and Yamada, 1982)
Land surface process	Xue et al. (1991, 1996); Dirmeyer and Zeng (1999)	Xue et al. (1991, 1996)
Shallow convection	Tiedtke (1984)	Tiedtke (1984)
Shortwave radiation	Briegleb (1992)	Briegleb (1992)
Diagnostic cloud fraction and optical properties	Kiehl et al. (1998)	Kiehl et al. (1998)

stratocumulus region. It was found that to understand the efficacy of a given change in this coupled model on the mean state and on the seasonal to interannual scales of variability, multidecadal integrations (over 50 yr) were required for the upper ocean to equilibrate.

V3.2 is now run at exactly the same resolution as the NCEP reanalysis model (T62L28; Kalnay et al., 1996) with identical topography. This was primarily done to conduct seasonal hindcasts with this AGCM using initial conditions taken from the NCEP reanalysis avoiding interpolation problems. The vertical coordinate system is the terrain following sigma coordinate. V2.2 is run at T42 horizontal spectral truncation with 18 terrain following sigma levels. The dynamical core is based on CCM3.6.6 (Kiehl et al., 1998) as in V2.2. Here, all prognostic variables except the moisture variable are treated spectrally. Moisture is advected by the Semi-Lagrangian scheme.

The outline of the physics of V3.2 is presented in Table 1 and compared with V2.2 of the model. For the planetary boundary layer (PBL) we have adopted the non-local scheme of Hong and Pan (1996). Local-K theory, on which the planetary boundary layer scheme of V2.2 is based, parametrizes turbulent mixing with an eddy diffusivity based on local gradients of wind and temperature. This has the potential to fail in unstable boundary layers because the influence of large eddy transports is not accounted for (Troen and Mahrt, 1986; Holtslag and Moeng, 1991). The non-local scheme following Hong and Pan (1996) parametrizes the counter-gradient transport effected through the large-scale eddies. The long wave scheme in V3.2 follows that of Collins et al. (2002) which was developed from water vapor line and continuum treatments that use a line-by-line radiative transfer model (GENLEN2) which is more accurate than the broad-band absorptance method used in V2.2. Although the deep convection is still the Relaxed Arakawa Schubert (RAS) scheme in V3.2, the determination of the fraction of the detrained cloud liquid water is done by means of an explicit budget equation in the cloud model (Bacmeister et al., 2000) in V3.2 instead of an empirical profile derived from GATE (Moorthi and Suarez, 1992) in V2.2. The land surface model follows the formulation of the Simplified Simple Biosphere (SSiB) scheme (Dirmeyer and Zeng, 1999) based on Xue et al. (1991, 1996). The version of SSiB in V3.2 was used in the second Global Soil Wetness Project (International GEWEX Project Office, 2002). Among the most significant differences from the earlier version (V2.2) is that the soil temperature and wetness are predicted in six layers (instead of three), with four embedded within the root zone. This provides a more consistent and realistic simulation of the decrease of transpiration with increasing soil moisture stress, preventing so-called 'stomatal suicide'. The fourth order horizontal diffusion coefficient was reduced by 2 orders of magnitude in V3.2 relative to V2.2. Second order horizontal diffusion was introduced in the top two layers of the V3.2 model to achieve numerical stability. Additionally, we have implemented a uniform calculation of saturation vapor pressure following Marx (2002) and allowed for variation of the latent heat of phase change with temperature following Bohren and Albrecht (1998) in V3.2.

2.2. The ocean model

The ocean model is version 3 of the Geophysical Fluid Dynamics Laboratory MOM (Pacanowski and Griffies, 1998). It uses a finite difference treatment of the primitive equations of motion using the Boussinesq and hydrostatic approximations in spherical coordinates. The domain is that of the world ocean between 74°S and 65°N. The coastline and bottom topography are realistic except that ocean depths less than 100 m are set to 100 m and the maximum depth is set to 6000 m. The artificial high-latitude meridional boundaries are impermeable and insulating. The zonal resolution is 1.5°. The meridional grid spacing is 0.5° between 10°S and 10°N, gradually increasing to 1.5° at 30°N and 30°S and fixed at 1.5° in the extratropics. There are 25 levels in the vertical, with 17 levels in the upper 450 m. The vertical mixing scheme is the non-local K profile parametrization of Large et al. (1994). The horizontal mixing of tracers and momentum is Laplacian. The momentum mixing uses the space-time dependent scheme of Smagorinsky (1963) and the tracer mixing uses Redi (1982) diffusion along with Gent and McWilliams (1990) quasi-adiabatic stirring.

3. Design of experiments

For the new coupled model simulation (V3.2-MOM3; hereafter NEW), the ocean model from the initial state of rest with intial conditions of temperature and salinity of Levitus (1982) was forced with climatological wind stress derived from special sensor microwave imager (SSMI) for a period of 100 yr. Thereafter, the model was integrated in the coupled system with earlier versions (V3.0 and V3.1) of the AGCM for a period of 80 yr. The coupled model (V3.2 + MOM3) was further integrated for 95 yr from such an initial state of the ocean. The results shown are computed using the last 70 yr of the integration discarding the first 25 yr as a spin-up period.

The coupled model (V2.2-MOM3; hereafter OLD) integration details follows from Kirtman et al. (2002). It is a 70 yr coupled run with the last 40 yr of the integration being shown here. The ocean initial state for this coupled run was spun up from an initial state of rest with initial conditions of temperature and salinity of Levitus (1982) forced with climatological wind stress from SSMI for a period of 100 yr.

4. Result

In discussing and validating the model results we use the Hadley Center Global Sea Ice and Sea Surface Temperature (HADISST, Version 1.1; Rayner et al., 2002; in the text interchangably used with observations) for monthly mean observed SST available at 1° resolution, NCEP-NCAR reanalysis (Kalnay et al., 1996)

made available on a 2.5° × 2.5° latitude–longitude grid for atmospheric variables, gridded precipitation on 2.5° × 2.5° latitude–longitude grid from the Climate Prediction Center Merged Analysis Precipitation (CMAP; Xie and Arkin, 1996) and an ocean data assimilation (ODA) analysis of available ocean observations following Rosati et al. (1997) for subsurface ocean quantities. All the results shown are computed from all calendar months unless mentioned otherwise. In computing climatological means, we use 40 (70) yr of the OLD (NEW) model integration, the last 70 yr (1930–2000) of HADISST, all 52 yr of the NCEP-NCAR reanalysis (1948–2000), 22 yr of the CMAP data (1979–2000), and 19 yr of the ODA (1980–1998). For the OLD run, we have stored only the atmospheric variables for the last 40 yr of the coupled integration. Therefore, the comparison between the OLD and the NEW coupled simulations will not include subsurface variables. The different duration of the analysis periods for the NEW and OLD simulations does not seem to be an issue. In fact, the results presented here for the NEW model did not change significantly when only 40 yr were used.

Although in this study we have concentrated on the seasonal to interannual variability of the ENSO phenomenon, longer time variations of ENSO (Gu and Philander, 1995; Wang, 1995; Timmermann, 1999) make such validation somewhat uncertain and can limit the understanding of the ENSO phenomenon from the available short records of observations. Model errors are larger than observational errors, so that inaccuracies in observations do not prevent the identification of model deficiencies.

4.1. Mean upper ocean and precipitation errors

In Figs. 1a and b, we show the mean annual SST errors (computed as the climatological mean difference of the annual mean SST between the simulation and the observations) in the tropical oceans from the OLD and the NEW coupled runs. The OLD (NEW) model has a warm (cold) bias in the equatorial Pacific region with a root mean square error of 3.91°(0.94°) and 3.19°(1.2°) over the Niño3 and Niño3.4 regions, respectively. In the OLD model, there was excessive downwelling shortwave at the surface (Schneider, 2002) that contributed to the warm bias in the equatorial Pacific Ocean. The error in the NEW model is typical of the models exhibiting the split-ITCZ problem. A vast improvement is observed from the OLD to the NEW coupled simulation even over the stratus region in the eastern tropical Indian, Pacific and the Atlantic Oceans. These errors over the equatorial Ocean and in the eastern Oceans are comparable to those in many of the IPCC models used in AR-4 (not shown; Covey et al., 2003; Guilyiardi, 2006).

The depiction of this mean error is intuitively important in evaluating the SST anomalies and precipitation anomalies associated with ENSO variability. This is further substantiated in Figs. 2a and b showing the climatological annual mean precipitation errors from the two simulations. These figures are consistent with climatogical annual mean SST errors (Figs. 1a and b), in that, for the most part at least in the OLD model the wet (dry) bias in precipitation follows the warm (cold) bias in SST errors. In the NEW model the dry bias over the central and eastern equatorial Pacific Ocean is straddled by a wet bias in both hemispheres as typical of the split ITCZ problem. It is interesting to note that a similar split ITCZ problem exists over the tropical Atlantic Ocean. The cold bias in the equatorial Pacific in the NEW model is accompanied by an easterly bias in the low level winds over the equatorial Pacific (not shown).

The mean error in the thermocline depth in the NEW model as assessed by the depth of the 20°C isotherm is shown in Fig. 3a.

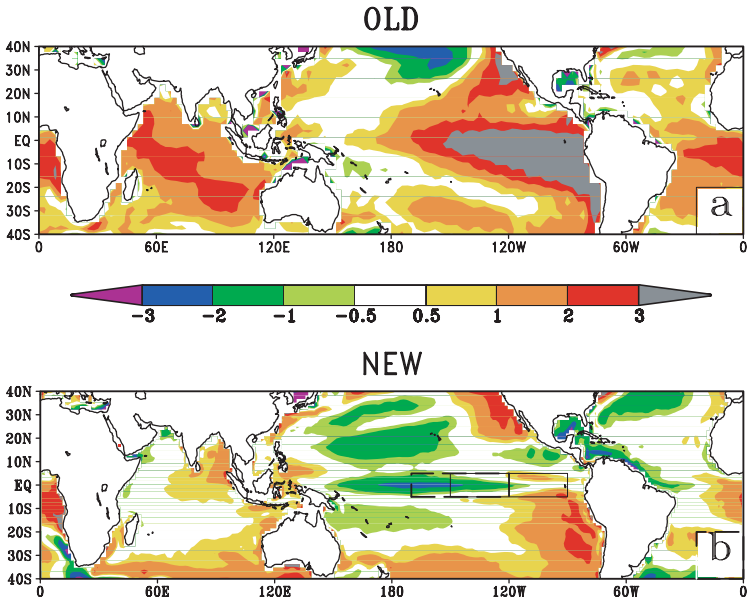

Fig. 1. The climatological annual mean errors of SST (in °C) from the (a) OLD and the (b) NEW coupled simulation. The outline of the Niño3 (Niño3.4) in solid (thick dashed line) is also shown.

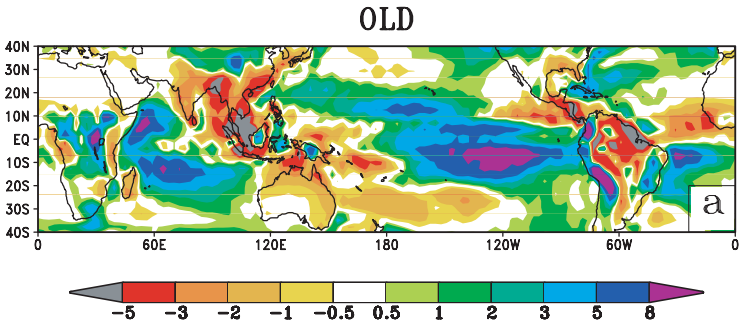

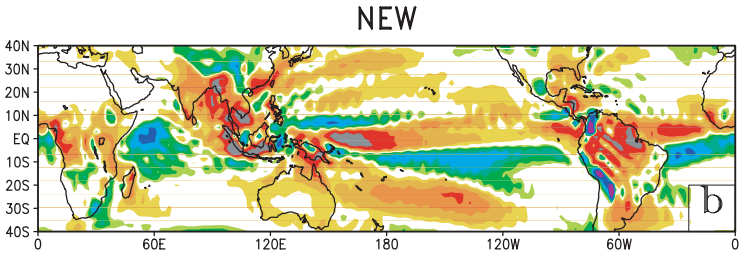

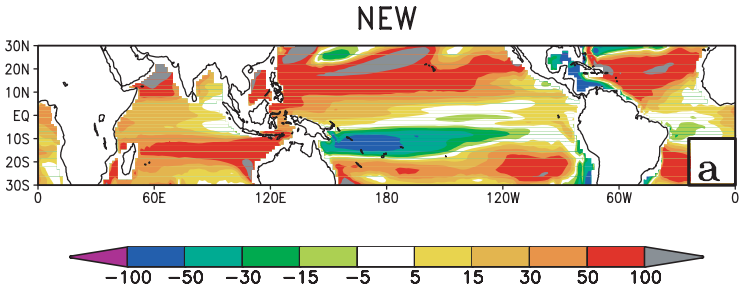

Fig. 2. Same as Fig. 1 but for precipitation. The units are in mm d^{-1}.

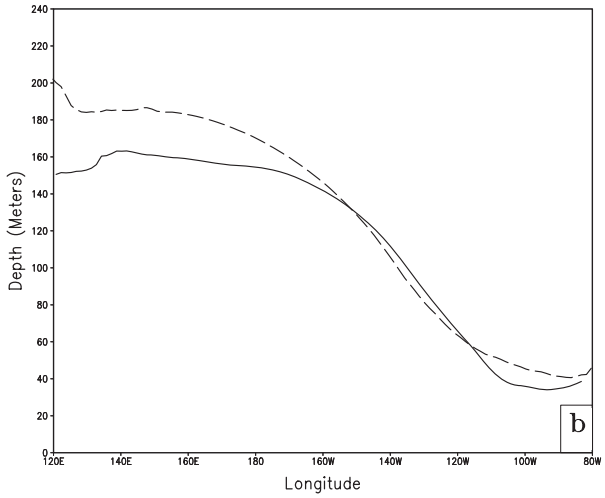

Fig. 3. (a) The annual mean errors of the thermocline depth (in meters) from the NEW model based on ODA (Rosati et al., 1997) over the tropical oceans. The thermocline depth is diagnosed from the depth of the 20°C isotherm. (b) The thermocline depth along the equatorial Pacific from the ODA (solid line) and the NEW coupled simulation (dashed line).

It is important indicator to gauge the errors in the thermocline depth, as the feedback of the subsurface ocean is an important of ENSO variability (Philander, 1983; Suarez and Schopf, 1988; An and Jin, 2001) The model clearly has a relative minimum of systematic error in the equatorial oceans straddled by the positive (negative) errors to the (north) south of the equator in the tropical Pacific and the Atlantic Oceans. The model tends to simulate a relatively deeper thermocline over the tropical Indian Ocean with respect to the ODA. The errors in the thermocline depth increase poleward of 5° latitude in either hemisphere over the tropical oceans.

The mean thermocline depth in the equatorial Pacific Ocean is shown in Fig. 3b for the NEW model simulation. The NEW model is able to capture the sharp zonal gradient in the

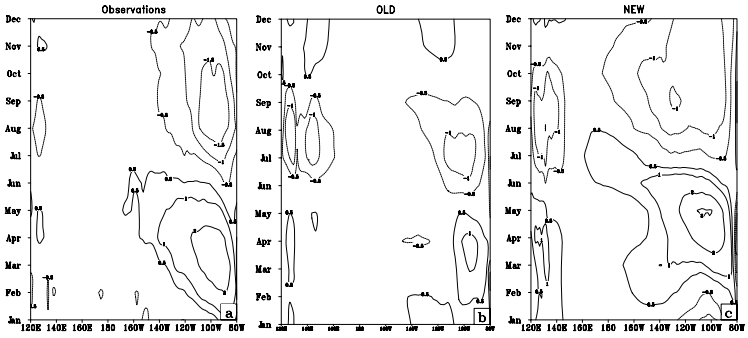

Fig. 4. The climatological annual cycle of SST in the equatorial Pacific Ocean from (a) observations (HADISST) the (b) OLD and (c) NEW coupled model simulation.

thermocline depth from the western Pacific where it is relatively deep to the eastern Pacific where it nearly shoals to the surface. This sharp gradient is found to be critical to the onset and phase locking of the ENSO (An and Jin, 2001; Jin, 1997).

4.2. *Mean annual cycle of the equatorial pacific sst and wind stress*

The successful simulation of both the mean annual cycle and the interannual variability in the tropics has proven to be surprisingly difficult in many CGCMs (Ineson and Davey, 1997). The climate drift in the mean annual cycle of SST in the tropics is a serious flaw in many of the CGCMs (Mechoso et al., 1995) that can have serious impacts on CGCM seasonal forecasts (Tziperman et al., 1997; Yang and Anderson, 2000).

In Figs. 4a–c, we show the climatological mean annual cycle of the equatorial Pacific SST from HADISST, OLD and the NEW coupled model simulations, respectively. As depicted in Fig. 4a, the observations show a distinct annual cycle over the eastern Pacific with the warmest (coldest) SST occurring in March–April (August–September). The OLD coupled model has a weaker annual cycle in the eastern Pacific with a hint of a semi-annual cycle. The NEW coupled model in Fig. 4c reproduces the observed mean annual cycle reasonably well. The westward migration of the warm SST in the early part of the year is also well simulated by the NEW model. However, the pronounced annual cycle in the far western Pacific Ocean simulated by both models is unrealistic. In addition, the cold (warm) SSTA in the boreal fall (spring) is smaller (larger) in amplitude in the NEW model relative to the observations.

In Figs. 5 and 6, we show the annual cycle of the zonal and the meridional wind stress from the NCEP reanalysis, OLD and NEW model simulations. In both of these figures the NEW model simulates the annual cycle of the wind stress (both zonal and meridional components) in the equatorial eastern Pacific Ocean in a way that conforms well with observations. The OLD model displays a distinct semi-annual cycle especially in the zonal wind stress (Fig. 5b). In addition, the zonal wind stress anomalies in the eastern Pacific in the OLD model is weaker than in the NEW model and NCEP reanalysis. However, both models exhibit stronger wind stress annual cycle over the equatorial western Pacific region compared to NCEP reanalysis. The large anomalies of the meridional wind stress in the OLD model (Fig. 6b) are farther westward from the eastern boundary contrary to NCEP reanalysis (Fig. 6a) and the NEW model (Fig. 6c). However, both models exhibit stronger wind stress annual cycle over the equatorial western Pacific region compared to NCEP reanalysis. But the stronger than observed meridional wind stress

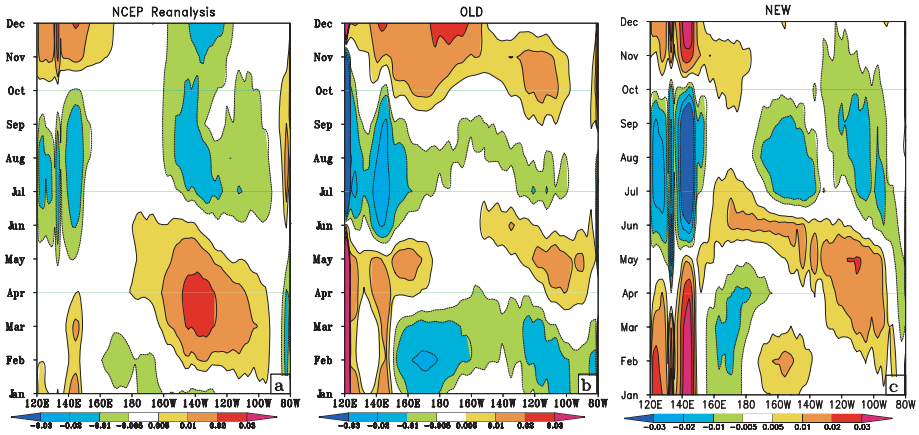

Fig. 5. Same as Fig. 4 but for zonal wind stress. The units are in N m^{-2}.

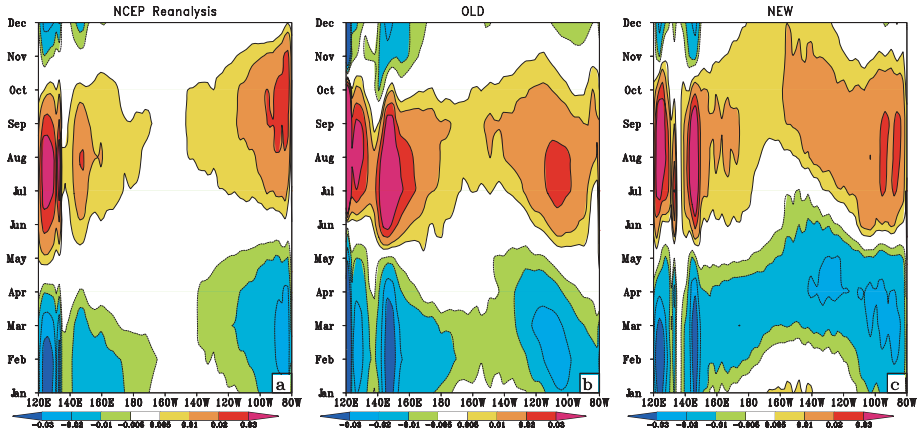

Fig. 6. Same as Fig. 4 but for meridional wind stress. The units are in N m^{-2}.

in both models over central equatorial Pacific reflects the strong meridional (Hadley-type) overturning in the coupled simulations as a result of the split ITCZ (Nigam et al., 2000).

4.3. *Temporal variability of Niño3 SST*

ENSO has a characteristic feature of having a broad peak in the range of 2–7 yr. This feature has been often validated in models by examining the sample spectrum of the Niño3 SST (Meehl and Arblaster, 1998). In Fig. 7, we show the Niño3 SST spectrum from both the observations (HADISST) and the coupled model simulations. HADISST displays a broad peak from 3 to 7 yr. The OLD (NEW) model has a characteristic feature of strong (weak) bi-ennial cycle. The strongest peak of the Niño3 SST spectrum in the NEW model is around 3 yr which just falls within the broad peak of the observed spectrum. However, compared to HADISST the sharpness of the spectrum in the NEW and the OLD model suggests that ENSO is relatively regular in the coupled simulations. Furthermore, both models exhibit insignificant low frequency (>4 yr) variability.

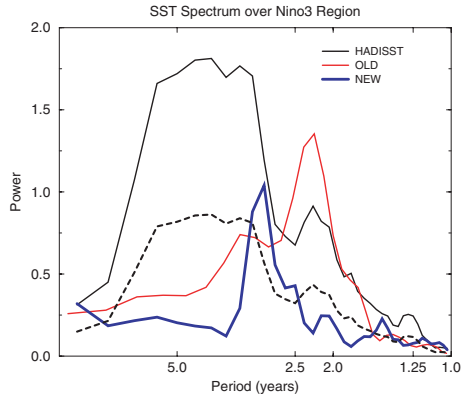

Fig. 7. The sample spectrum of SST over the Niño3 region is shown from observations (HADISST) and the coupled simulations. The dashed line in the figure shows the lower limit of the 95% confidence interval of the observed sample spectrum for 4° of freedom according to chi-squared test. The upper limit of the confidence interval is not shown for clarity. Niño3 SST at different lead times. The autocorrelation of first order autoregressive process (in red) is also shown.

4.4. *Seasonal phase locking of the Niño3 SST variability*

The apparent phase locking of ENSO events to the mean annual cycle in the eastern equatorial Pacific with a tendency to peak at the end of the calendar year is perhaps one of ENSO's most distinctive characteristics (Rasmusson and Carpenter, 1982). ENSO variability typically peaks in boreal winter and diminishes in boreal spring with relatively weak variability in the boreal summer and early fall. In Fig. 8, we show the monthly standard deviation of the SST anomalies in the Niño3 region from the observations and the two coupled model simulations. It is apparent from the figure that the NEW coupled model in contrast to the OLD model has a preference for relatively high variability in the winter season, as observed. However, the standard deviations in the NEW simulation are much smaller than observed. It should however

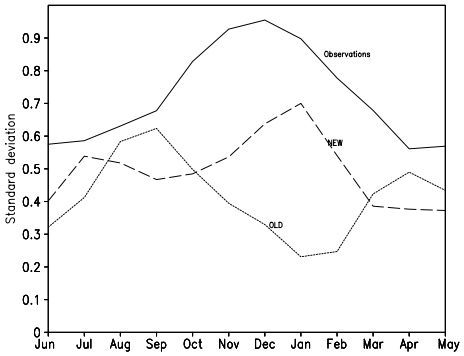

Fig. 8. The standard deviation of SST over the Niño3.4 region from observations (HADISST; solid line), the OLD (short dashed line) and the NEW (long dashed line) model simulations.

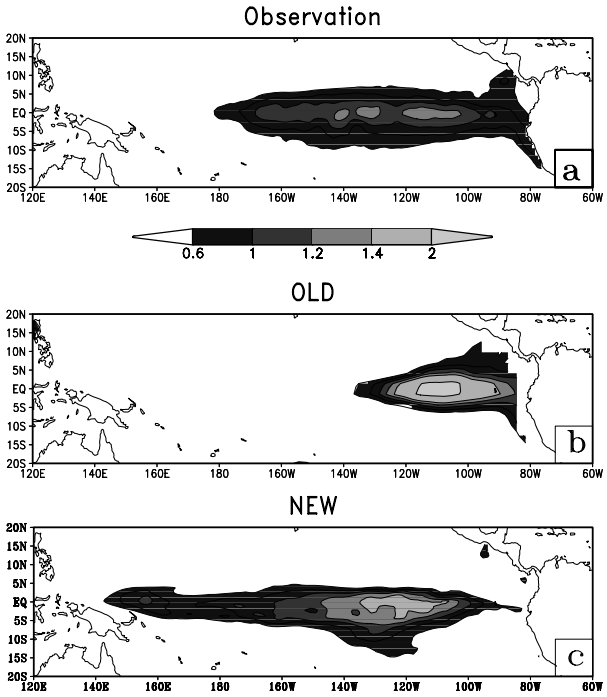

Fig. 9. The regression of the Niño3 SST index on tropical SST from (a) Observations (HADISST) the (b) OLD and (c) NEW coupled model simulations. Only values significant at the 90% confidence interval according to the *t*-test are plotted.

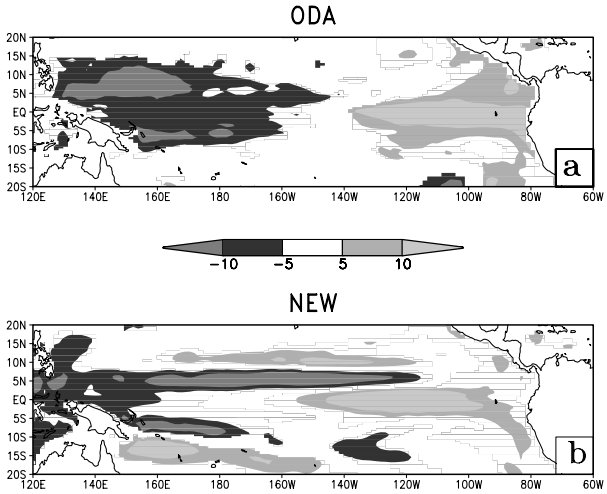

Fig. 10. The regression of the Niño3 SST index on the thermocline depth (in meters) in the tropical Oceans from (a) the ODA and (b) the NEW model simulation. Only values significant at the 90% confidence interval according to the *t*-test are plotted.

be noted that the peak variability of some ENSO events does not necessarily occur in the preferred boreal winter season. In summary, the NEW model is an improvement over the OLD model in terms of ENSO's phase locking to the annual cycle.

4.5. ENSO related SST and upper ocean variability

The spatial structure of the anomalous SST and upper ocean variability plays a significant role on the extra-tropical response (Hoskins and Karoly, 1981; Kumar and Hoerling, 1998; Chen, 2004). Regressions of the Niño3 SST index on tropical Pacific SST from the observations and the OLD and the NEW coupled model simulations are shown in Figs. 9a–c, respectively. The NEW model simulation reproduces the observed SST variability over the eastern equatorial Pacific comparatively well. But the NEW model has a tendency to produce too much variability in the western Pacific. The OLD model displays variability that is spatially confined to the eastern Pacific which does not extend into central Pacific Ocean. In contrast, the NEW model produces excessive variability over the western Pacific Ocean. Furthermore, the NEW model and the OLD model have a tendency to produce too little variability along the coastline of Peru.

The cycle of interactions involved in ENSO include changes in the thermocline depth (Philander, 1983) with shoaling (deepening) in the western (eastern) equatorial Pacific Ocean. SSTA are the manisfestation of an ENSO event while the thermocline depth anomalies act as precursors and also mark the end of a ENSO event (Zelle et al., 2004). In Figs. 10a and b, we have plotted the regression of the Niño3 SST index on the corresponding thermocline depth from the ODA and the NEW coupled simulation, respectively. Both show a dipole like structure between the eastern and western equatorial Pacific Ocean that fits the standard schematic of ENSO (Philander, 2001). Furthermore, the magnitude of variability of the simulated thermocline depth in the eastern Pacific is comparable to the ODA. However, it should be noted that the meridional scale of the thermocline depth anomalies in the NEW model is smaller than in the ODA.

In Figs. 11a and b, we show the regression of the Niño3 SST index on the thermocline depth at a lag of 8 months (Niño3 SST index lagging) from the ODA and the NEW model simulation, respectively. Meinen and McPhaden (2000) have highlighted the importance of this variability which has anomalies of the same sign along the equatorial Pacific that describes the variations of the zonally averaged thermocline depth on the SST variations. Following the 'recharge oscillator' paradigm Jin (1997), the SST anomaly in the eastern equatorial Pacific is approximately in quadrature with the phases of maximum variations of zonally averaged thermocline depth. Therefore, this pattern of the thermocline depth acts as a precursor to the Niño3 SST variations (Meinen and McPhaden, 2000). Here (Fig. 11) we identify this variation at a lag of 8 months in the ODA and the NEW model simulation. It is seen that the variations of the thermocline depth are much smaller than in Fig. 10 which is consistent with the diagnosis of Meinen and McPhaden (2000) and Capotondi et al. (2006) who identified this variability as the second EOF mode

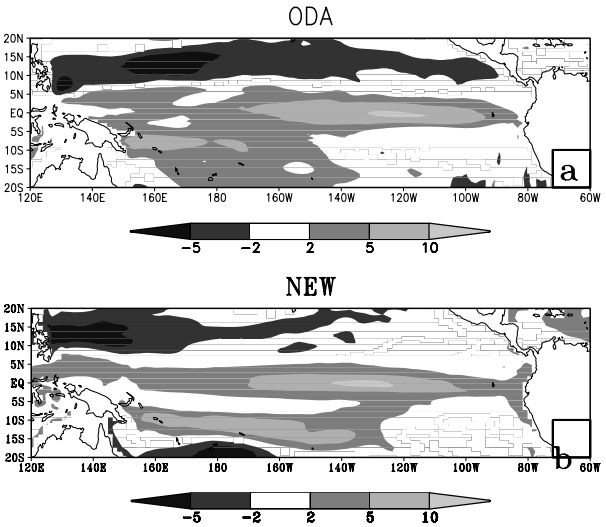

Fig. 11. Same as Fig. 10 but with Niño3 SST index lagging the thermocline depth by 8 months.

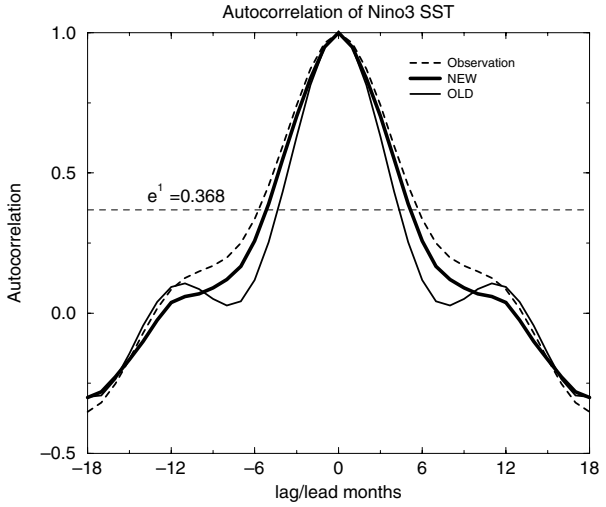

Fig. 12. The autocorrelation of the Niño3 SST index from observation (HADISST) and the coupled simulation. Horizontal line is drawn at $e^{-1} = 0.368$ to estimate the duration of the event during one phase of the ENSO cycle.

explaining about one-fifth of the total variance. The NEW model simulation shows a close resemblance to ODA in this feature.

4.6. Duration of ENSO events

Following the methodology proposed in Joseph and Nigam (2006) we show in Fig. 12 the autocorrelation of the Niño3 SST at various leads and lags. The width of the autocorrelation curve at its intersection with e^{-1}(decorrelation values; =0.368) line provides an estimate of the duration of the event in any one phase (warm or cold). The width in the observations is about 14 months while in the NEW (OLD) model simulation it is around 13 (10) months. The change in sign of the autocorrelation curve signifies the connectivity to the opposite phase of variability (Joseph and Nigam, 2006).

4.7. Evolution of SST in the equatorial pacific

Many coupled models have a tendency of being in a state of perpetual ENSO, that is, one event of ENSO would lead to the other. This leads to the absence of neutral events in such models. This is often seen when the duration of the ENSO events are comparable to half the time period of the spectral peak.

In Figs. 13a–c, we display the lag/lead regression of the Niño3 SST with the equatorial Pacific SST over a 42 month interval from both the observations and the two coupled model simulations, respectively. Positive lag indicates that the Pacific SST leads the standardized Niño3 SST index. The observations show an asymmetry in the evolution of equatorial SST with the SST anomalies being larger and slightly shorter in one phase of the evolution relative to the other. The OLD model has a strong biennial cycle with duration of ENSO events typically around 10 months (Fig. 12) that puts it in a perpetual ENSO mode. The evolution of equatorial Pacific SST is rather well captured by the NEW coupled model besides the east-west coherent structure of the SST anomalies. However, the NEW coupled model extends its warm SST anomalies too far to the west relative to the observations.

4.8. Evolution of the subsurface ocean temperatures in the equatorial pacific

In Fig. 14, we show the regression of the Niño3 SST index on the equatorial subsurface ocean temperatures at 12, 8, 4, 0 and -4 months lead from the ODA and the NEW model simulation. In this figure the standardized Niño3 SST index lags the equatorial Pacific subsurface ocean temperature anomalies at positive lags. In order to make the discussion more lucid in reference to this figure we make an assumption that negative (positive) values correspond to cold (warm) Niño3 SST index events. It is apparent from the figure that the upper ocean anomalies before, during and after the evolution of the warm ENSO event, in the coupled model compare well with the ODA. At 12 months preceding the warm ENSO event (Figs. 14a and f) the warm anomalies from the west Pacific are shown to move eastward as the cold upper anomaly in the east Pacific recedes. Further, at 8 months (Figs. 14b and g) lead to the ENSO event, the anomalies gain magnitude and the eastward tilt with decreasing depth becomes more prominent. At 4 months prior to the ENSO event (Figs. 14c and h), the warm anomalies are established in the east Pacific while cold anomalies appear in the ODA in the West Pacific. At zero lag (Figs. 14d and i) the anomalies in the east and west Pacific become larger and extend deeper in the upper ocean. At 4 months (Figs. 14e and j) past the ENSO event the warm anomalies in the east Pacific begin to retreat in the east Pacific

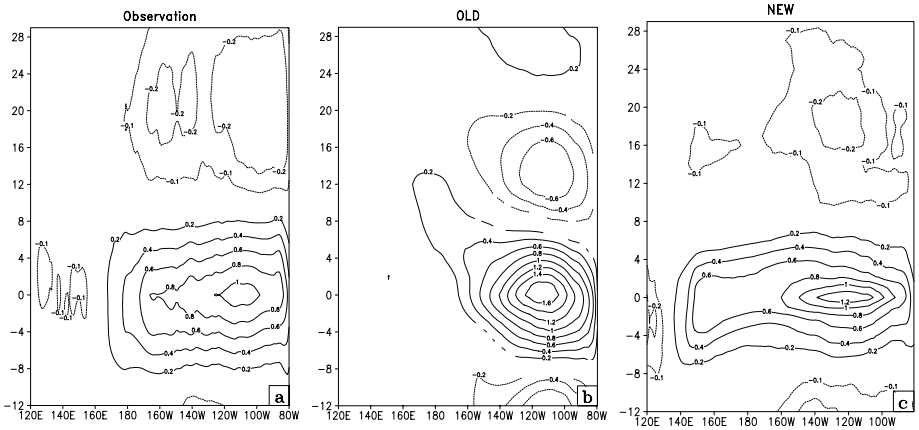

Fig. 13. Lead/lag Niño3 SST index regressions on equatorial Pacific SST fro m (a) Observations (HADISST) (b) the OLD and (c) the NEW coupled model simulations. At positive lags the Niño3 SST index lags the equatorial Pacific SST. Only values significant at the 90% confidence interval according to the *t*-test are plotted.

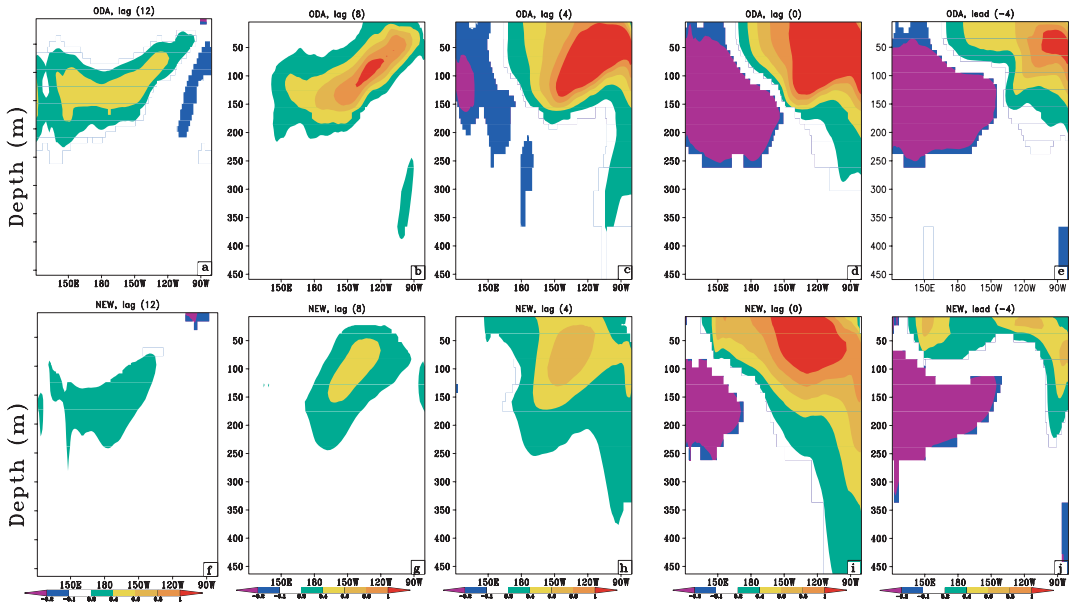

Fig. 14. The regression of Niño3 SST index on the equatorial subsurface ocean temperatures from the ocean data assimilation (Rosati et al., 1997) and the NEW coupled model simulation at (a), (f) 12 months lag, (b), (g) 8 months lag (c), (h) 4 months lag, (d), (i) 0 months lag and (e), (j) 4 months lead. At positive lags Niño3 SST index lags the subsurface ocean temperature anomalies. Only values significant at the 90% confidence interval according to the *t*-test are plotted.

while the cold anomalies from the west Pacific propogate further eastward. Despite the reasonable simulations of the subsurface ocean temperature anomalies, a glaring disparity in the NEW model simulation is its weaker amplitude of the variability at all lag/lead times.

4.9. *Relationship of the Niño3 SST variability with the tropical oceans*

This ENSO metric is extremely important to validate given that the intrinsic variability in the tropical Atlantic and the Indian Oceans is comparable to that due to the remote ENSO forcing (Chang et al., 2003; Krishnamurthy and Kirtman, 2003). It should be noted that these correlations over the Indian and the Atlantic Oceans are seasonally dependent and involve lead-lag relationship with the Niño3 SST variability. However, these relatioships are so dominant that they are reflected when all calendar months are taken into consideration as shown below.

In Fig. 15, we show the contemporaneous correlation of the Niño3 SST index with global tropical SST. The horse-shoe pattern of the correlation in the tropical Pacific that is evident in the observations is simulated by the NEW model simulation while

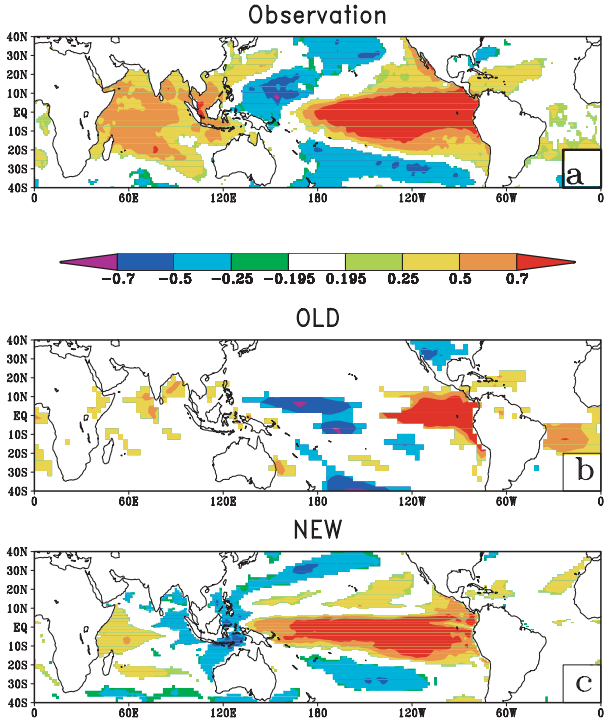

Fig. 15. Contemporaneous correlations of Niño3 SST with global tropical oceans from (a) Observations (HADISST), (b) the OLD and (c) the NEW coupled simulations. Only values significant at the 10% significance level according to the *t*-test are shown.

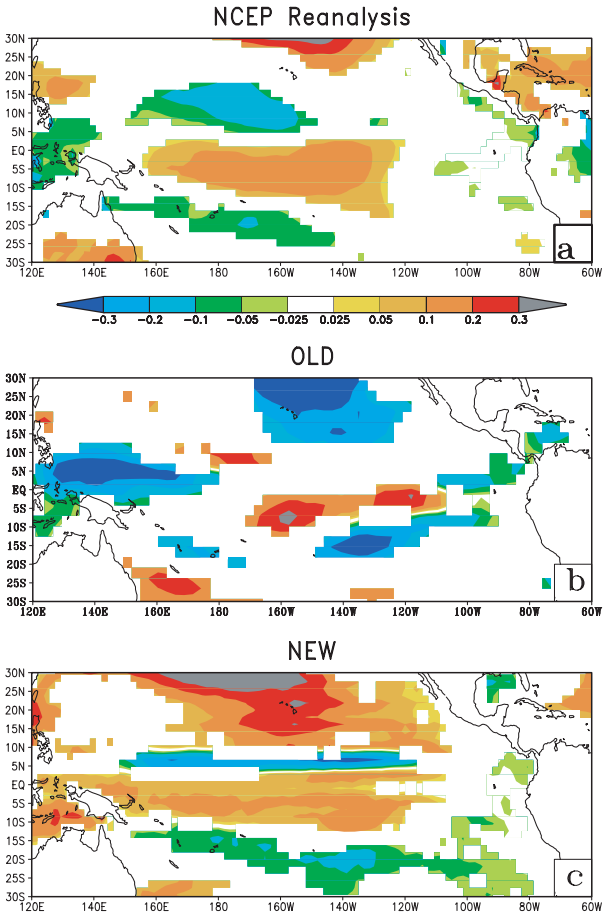

Fig. 16. The regression of the Niño3 SST index on the zonal wind stress anomalies from the (a) NCEP reanalysis, (b) the OLD and (c) the NEW coupled simulation. Only values significant at the 90% confidence interval according to the *t*-test are plotted. The units are in dynescm^{-2}.

it is not captured in the OLD simulation. In the tropical Atlantic, the correlations are weaker but significant verifiable positive correlations appear in the Carribbean Sea in both simulations. These correlations over the northern tropical Atlantic region peak in the boreal spring following the ENSO peak in the preceding winter (Enfield and Mayer, 1997; Huang, 2004).

However, the OLD model is able to capture the positive correlation albeit stronger than observations over the South tropical Atlantic Ocean which is completely missed by the NEW model. This variability over the southern Atlantic Ocean forced by ENSO also appears in the Boreal spring but is found to be much weaker in observations than that over the North tropical Atlantic Ocean (Huang, 2004).

In the western Indian Ocean, the positive correlations are well (poorly) represented by the NEW (OLD) coupled model. However, the negative correlations in the eastern Indian Ocean appear unrealistic in the NEW model. Since the ENSO variability is relatively weak in the NEW model, the dominant basin wide positive correlations of the tropical Indian Ocean with Niño3 SST variability is not well simulated. Another problem that the NEW model displays in this figure is the increased variability over the western Pacific Ocean. Some of the other IPCC (AR4) models also suffer with such a bias (Joseph and Nigam, 2006).

4.10. Relationship between Niño3 SST and wind stress

The relationship between Niño3 SST and wind stress represents the coupled air–sea interaction of ENSO. The Bjerknes feedback mechanism (Bjerknes, 1969) which relates tropical ocean adjustment (involving deepening of thermocline and weakening of equatorial upwelling) in response to modulations in the low level trade winds (development of westerly wind anomaly) that follows from the shift of the Walker circulation eastward, is reflected in this relationship. Besides, as shown in Kirtman (1997), the meridional structure of the wind stress anomaly has a bearing on the ENSO period as a result of role played by the off equatorial Rossby waves.

In Figs. 16a–c, we show the regression of the Niño3 SST index on the zonal wind stress anomalies from the NCEP reanalysis, the OLD and the NEW model simulations, respectively. The reanalysis clearly shows a coherent westerly wind stress anomaly over the warm pool region in the western Pacific that is stradled

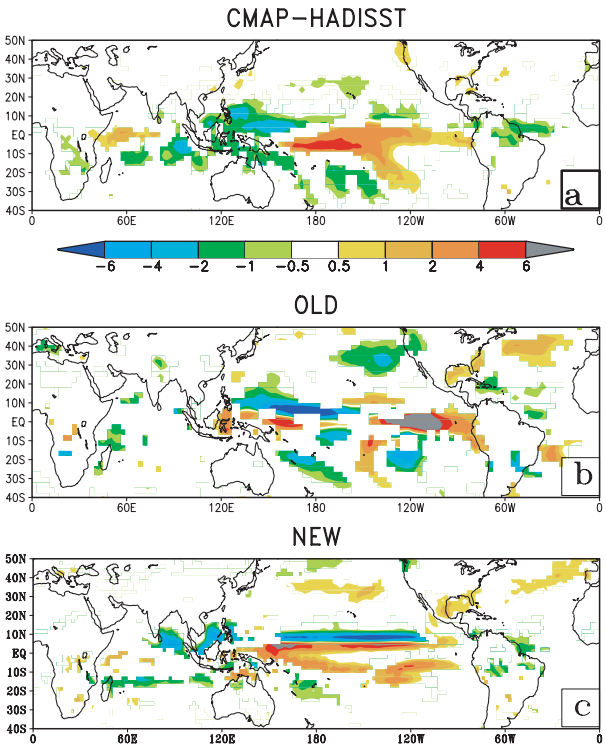

Fig. 17. The regression of the Niño3 SST index on precipitation from (a) Observations (SST from HADISST and precipitation from CMAP), (b) the OLD and (c) the NEW coupled simulations. Only values significant at the 90% confidence interval according to the *t*-test are plotted. The units are in mm d^{-1}.

by anomalies of the opposite sign in both hemispheres. This is reasonably well captured by the NEW model simulation in Fig. 16c except that the wind stress anomaly in the warm pool region is narrower than the reanalysis and the anomalies off the equator especially in the north tropical Pacific is too meridionally confined. In addition, the wind stress anomalies from the subtropics extend too far to the south. In contrast, the variability of windstress in the OLD model is unrealistic over the whole domain.

4.11. Relationship between Niño3 SST and precipitation

In Figs. 17a–c, we show the regression of the Niño3 SST index on the precipitation from observations (CMAP and SST is from HADISST) and the OLD and the NEW model simulations, respectively. It should be noted that the reanalysis precipitation is sensitive to the model convective parametrization scheme (Nigam and Chung, 2000) and therefore is not used here for validation. In Fig. 17a, we have used 22 yr of CMAP precipitation extending from 1979 to 2000 with corresponding SST from the HADISST dataset.

The OLD model displays precipitation anomalies in the tropical Oceans which is at variance with the observed anomalies. The NEW coupled model simulation in Fig. 17c shows a verifiable modulation of precipitation over the central and eastern equatorial Pacific Ocean. The rainfall variability over the tropical north Atlantic is simulated albeit weakly. The split ITCZ phenomenon in the tropical Pacific is clearly seen in the NEW model simulation with the precipitation anomalies too meridionally confined suggesting a strong Hadley-like circulation. The figure also shows a general agreement between the simulation and the observations in the Indo-Pacific sector, southern Indian Ocean, and in the south Pacific convergence zone. However, the warm pool region shows enhanced rainfall anomalies in the simulation (that is unsupported by observations), which is consistent with the increased SST variance (cf. Fig. 9c) that extends too far to the west.

4.12. Mid-latitude atmospheric response to ENSO

The mid-latitude response to anomalous tropical heating due to ENSO is illustrated from the geopotential height anomalies of the mid-upper troposphere. Horel and Wallace (1981) showed that the equatorial convection forces a train of stationary Rossby waves that arc across the Pacific-North American on a great-circle route.

In Figs. 18a–c the regression of Niño3 SST index on 200 hPa geopotential height anomalies for December–January–February (DJF) are shown from the NCEP reanalysis and the OLD and the NEW model simulations, respectively. The NEW model simulation roughly resembles the SST forced pattern illustrated in Straus and Shukla (2000; cf. their Fig. 18a) that has broad centres around 45°N between 140°W and 160°E, between (and just west of) the Great Lakes and Hudson Bay and over the Gulf of Mexico (near 30°N). The rather zonally symmetric height response of the OLD model (18b) is contrary to the NCEP reanalysis in 18a. However, it should be noted that the ENSO variability is relatively weaker in the NEW model, apparent from the weaker height anomalies in the tropics in Fig. 18c.

5. Summary and discussion

In summary, the NEW COLA coupled climate model (COLA AGCMV3.2-MOM3) is comparable to many of the state of the art IPCC (AR4) models in its ENSO simulation (see Capotondi et al., 2006; Joseph and Nigam, 2006; Rao and Sperber, 2006). The climatological annual cycle of SST and wind stress in the eastern equatorial Pacific Ocean, the climatological annual mean zonal gradient of the thermocline along the equatorial Pacific Ocean, realistic evolution of ENSO percieved from subsurface ocean variability, prevalence of neutral events, and the seasonal phase locking of ENSO to the annual cycle are some of the major improvements in the ENSO simulation of the NEW coupled climate model relative to the OLD model.

This study also attempts to understand how such an improvement in the ENSO simulation occurred in the NEW model

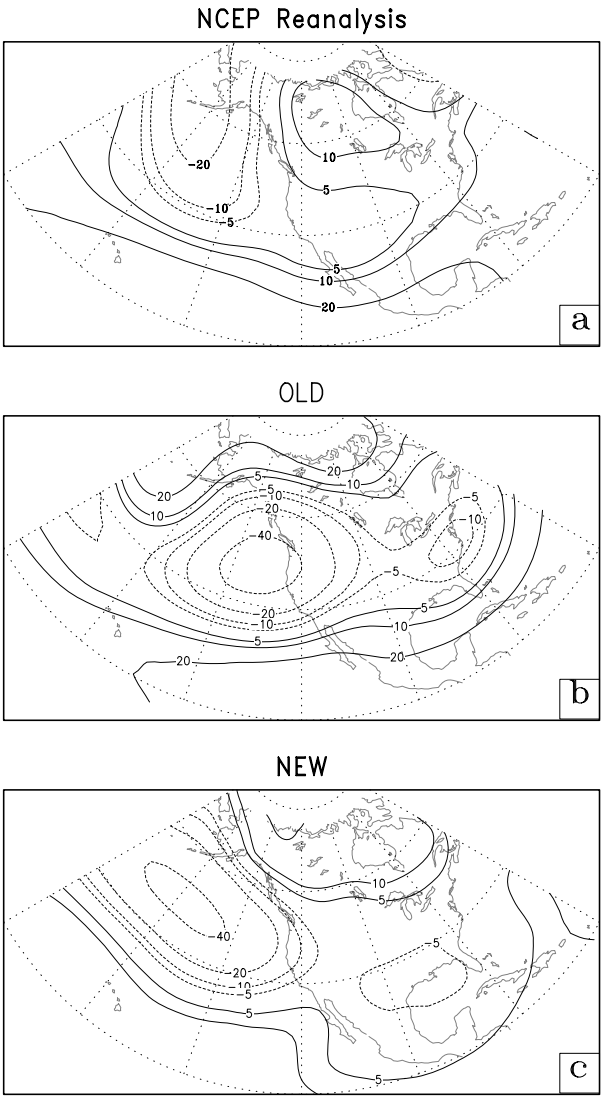

Fig. 18. The regression of the DJF Niño3 SST index with contemporaneous geopotential height (in meters) at 200 hPa from (a) the NCEP reanalysis (b) the OLD and (c) the NEW coupled model simulations.

relative to the OLD. It is rather difficult to isolate a process for the overall changes in the ENSO simulation of the NEW model from the OLD model given that a number of changes were made to the physical parametrization schemes and the numerics that included changes to the vertical discretization and horizontal diffusion to the AGCM of the NEW coupled model. Furthermore, Schneider (2002) showed that differences in the simulation over the eastern equatorial Pacific Ocean between two different coupled climate models could not be isolated to a dominant process in their atmospheric components. However, he showed (as seen in this study with identical ocean in the OLD and the NEW coupled models) that the differences in the atmospheric models are the prime drivers for the differences in the coupled simulations.

Table 2. The centre of mass (C) of the regressed wind stress from Fig. 16 calculated following Capotondi et al. (2006) as $C = \frac{\int_0^{l_x} \overline{\tau^x}(x)x\,\mathrm{d}x}{\int_0^{l_x} \overline{\tau^x}\,\mathrm{d}x}$ where, l_x is the width of the ocean, x is the longitude and $\overline{\tau^x}$ is the anomalous zonal wind stress averaged between 2°S and 2°N at each longitude

NCEP reanalysis	OLD	NEW
164°W	Undefined	176°E

Additionally, we contend that intercomparing schemes in coupled climate models for the purposes of evaluating its efficacy in reproducing the observed mean and variable climate is futile as long as tunable parameters are present.

However, based on our current understanding from several theoretical, observational and coupled modelling studies we provide some physical explanations for the differences in the ENSO simulation between the OLD and the NEW model. The ENSO time scale increased to 3 yr (Fig. 7) in the NEW model primarily because of the broadening of the meridional scale of the zonal wind stress anomalies (Fig. 16) over the Central Pacific. Kirtman (1997) has shown that such broadening of the wind stress excites the slower off-equatorial Rossby waves which result in a longer time period for the phase reversal of the ENSO cycle. Another complimentary theory is that the zonal location of the zonal wind stress anomaly can play a significant role in the ENSO period (An and Wang, 2000). Following Capotondi et al. (2006) we have calculated the centre of mass of the regressed wind stress from Fig. 16 for the NCEP reanalysis, NEW and OLD model simulations (Table 2). It is seen from Table 2 that the NEW model's centre of mass for the regressed wind stress is eastward and closer to NCEP reanalysis than the OLD model. In the OLD model the zonal wind stress anomalies are in fact outside the 2°S–2°N latitude band as a result of which the centre of mass is undefined. Following the argument of An and Wang (2000) which suggests that eastward shift of the zonal wind stress anomalies results in the increased contribution of the zonal feedback term in the SST tendency equation to growth of the ENSO cycle rather than its transition from one phase to the other also justifies the NEW model's increased ENSO period.

The improvement in the seasonal phase locking of ENSO arises from the improvement in the mean seasonal cycle of the SST and the associated thermocline variability. Meinen and McPhaden (2000) showed from subsurface observations that the contemporaneous zonal tilt and the zonally averaged thermocline depth variations at quadrature with the SST variability in the eastern Pacific are the two most dominant modes of the upper ocean water volume that dictate the evolution and sustenance of ENSO. Both these leading modes of the thermocline depth (Figs. 10 and 11) are qualitatively similar in the NEW model and ODA.

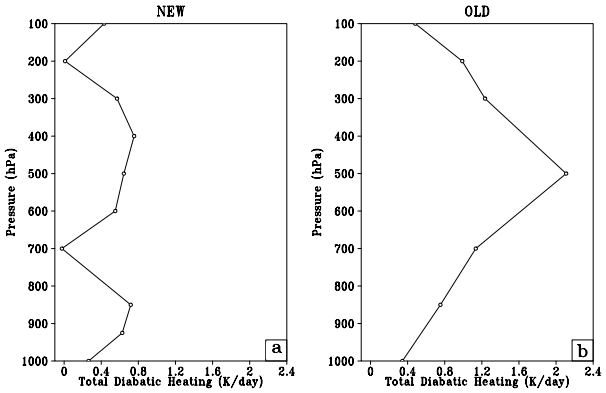

Fig. 19. The climatological area average (140°E–80°W and 10°S–10°N) annual mean total diabatic heating profile from the (a) NEW and (b) the OLD coupled model simulations.

Surface wind stress is an important source of thermocline variability and in the maintenance of its mean state. A significant improvement in the NEW model relative to the OLD model is seen in the mean annual cycle of the wind stress (Figs. 5 and 6) and its variability (Fig. 16). Nigam et al. (2000) from their linear diagnostic modelling study show that the spatial distribution and the vertical profile of diabatic heating have a profound influence on the surface wind anomalies. They argue from their diagnostic modelling study that a 'bottom heavy' heating profile will entail stronger low level prevailing winds. The improvement in the wind stress simulation of the NEW model is largely attributed to the change in the total diabatic heating profile shown in Fig. 19. In Fig. 19(a,b) it is clearly seen that the NEW (OLD) model heating profile is bottom (top) heavy. Furthermore, the diabatic heating profile of the NEW model (Fig. 19a) is qualitatively and quantitatively quite similar to the corresponding profile of the ECMWF reanalysis (cf. fig. 8 of Nigam and Chung, 2000).

On the other hand Nigam and Chung, (2000) and Nigam and Chung, (2000) argue that the strong diabatic cooling in the off-equatorial tropics from a more Hadley-like heating redistribution (as in most coupled climate models) result in an easterly bias of the surface winds. A similar feature of strong meridional gradient of heating is seen in Fig. 17c. This pattern is nearly identical when precipitation anomalies are replaced with total diabatic heating in both the OLD and the NEW models (not shown). The more east-west orientation of the heating in the OLD model (Fig. 17b) is probably one of the few positive features of the ENSO simulation in the OLD model.

6. Conclusions

In this study, we presented 12 salient observed features of ENSO to validate a coupled climate model for its ENSO simulation. Although, these features may not be exhaustive, they are sufficient to make a quantitative judgement on the veracity of the ENSO simulation, based on our present understanding of the phenomenon.

A long term simulation of the newly developed COLA coupled climate model was verified for these 12 features and contrasted with an older version of the COLA coupled model. Overall, the NEW coupled model is a major improvement over the OLD model. A summary of the results is presented in Table 3.

A fundamental difference, besides the differences in the ENSO features, between the OLD and the NEW model simulations is the shift from the warm SST bias in the equatorial Pacific to a cold SST bias. This is of great relevance to many current state of the art coupled climate models that suffer from a cold bias and concomitant easterly bias in the zonal wind stress over the equatorial Pacific. This difference between the OLD and the NEW model cannot be isolated to a single physical process in the atmosphere, land or in the ocean. We contend that the improvement seen in the total diabatic heating profile has significantly contributed to the overall improvement of the NEW model. If we follow the argument of Nigam and Chung, (2000), who relate the vertical heating distribution to bias in the surface wind stress and reconcile that surface wind stress is critical for the thermocline variability (without discounting the role of the net heat and fresh water fluxes under weak wind conditions) in the deep tropics, then a clear relationship can be noticed in how diabatic processes are critical for the simulation of the tropical climate

Table 3. A short summary of comparison between the OLD and the NEW COLA coupled climate models

Feature	OLD	NEW
RMSE of SST in the Niño3 region	3.91°	0.94°
Period of ENSO (determined from Niño3 SST spectrum	Biennial	3 yr
Seasonal phase locking of ENSO	Inexistent	Exists
Duration of ENSO events	10 months	13 months
Wind stress	Erroneous (biennial feature in zonal wind stress)	Verifiable
Subsurface ocean	Not analyzed	Reasonable
ENSO teleconnections	Poor	Relatively improved

(including its variability). However, it should be recognized that diabatic processes in the atmosphere (at least in the deep tropics) is a result of coupled interactions and therefore cannot be isolated to a process in a single component model. An important realization of this study is that the development of the coupled climate model should occur in a coupled framework and not in the isolation of the component models.

7. Acknowledgments

The authors would also like to express their deep appreciation to Drs. Byron Boville, William Collins of NCAR, Masao Kanamitsu of UCSD, Song-You Hong of Yonsei University, Shrinivas Moorthi of NCEP, Julio Bacmeister of NASA and Ben Cash of COLA for their invaluable suggestions at critical times of the development of the COLA AGCM. We would also like to acknowledge that comments from three anonymous reviewers helped us considerably in improving the content of this manuscript. This study was supported by NSF grant ATM0332910, NASA grant NNG04GG46G and NOAA grant NA04OAR4310034. The authors would also like to acknowledge the support of the computing infrastructure provided by the National Center for Atmospheric Research computing systems laboratory.

References

An, S.-I. and Wang, B. 2000. Interdecadal change of the structure of the ENSO mode and its impact on the ENSO frequency. *J. Climate* **13**, 2044–2055.

An, S.-I. and Jin, F.-F. 2001. Collective role of thermocline and zonal advective feedbacks in the ENSO mode. *J. Climate* **14**, 3421–3432.

Alexander, M. A., Blade, I., Newmann, M., Lazante, J. R., Lau, N.-C. and co-authors. 2002. The atmospheric bridge: the influence of enso teleconnections on air-sea interaction over the global oceans. *J. Climate* **15**, 2205–2231.

Bacmeister, J. T., Pegion, P. J., Schubert, S. D. and Suarez, M. J. 2000. An atlas of seasonal means simulated by the NSIPP-1 atmospheric GCM. **17**, NASA Tech. Memo-2000–104606, Goddard Space Flight Center, Greenbelt, MD (194 pp).

Bohren, C. F. and Albrecht, B. A. 1998. *Atmospheric Thermodynamics.* Oxford University Press, New York, 402 pp.

Bjerknes, J. 1969. Atmospheric teleconnections from the equatorial Pacific. *Mon. Wea. Rev.* **97**, 820–829.

Briegleb, B. P. 1992. Delta-Eddington approximation for solar radiation in the NCAR Community Climate Model. *J. Geophys. Res.* **97**, 7603–7612.

Capotondi, A., Wittenberg, A. and Masina, S. 2006. Spatial and temporal structure of Tropical Pacific interannual variability in 20th century coupled simulations. Ocean Modeling, **15**, 274–298.

Chang, P., Saravanan, R. and Ji, L. 2003. Tropical Atlantic seasonal predictability: the roles of El Niño remote influence and thermodynamic air-sea feedback. *Geophys. Res. Lett.* **30**, 1501–1504.

Chen, W. Y. 2004. Significant change of extratropical natural variability associated with tropical ENSO anomaly. *J. Climate* **17**, 2019–2030.

Collins, W. D., Hackney, J. K. and Edwards, D. P. 2002. An updated parameterzation for infrared emission and absorption by water vapor in the National Center for Atmospheric Research Community Atmosphere Model. *J. Geophys. Res.* **107**(D22), doi:10.1029/200/JD0011365, 2002.

Covey, C., Achuta Rao, K. M., Cubasch, U., Jones, P., Lambert, M. E. and co-authors. 2003. An overview of results from the coupled model intercomparison project (CMIP). *Global Planet. Change* **37**, 103–133.

Dirmeyer, P. A. and Zeng, F. J. 1999. Precipitation infiltration in the simplified SiB land surface scheme. *J. Meteor. Soc. Japan* **78**, 291–303.

DeWeaver, E. and Nigam, S. 2004. On the forcing of ENSO teleconnections by anomalous heating and cooling. *J. Climate* **17**, 3225–3235.

Enfield, D. B. and Mayer, D. A. 1997. Tropical atlantic sea surface temperature variability and its relation to El Niño southern oscillation. *J. Geophys. Res.* **102**, 929–945.

Gent, P. R. and McWilliams, J. C. 1990. Isopycnal mixing in ocean circulation models. *J. Phys. Oceanography* **25**, 150–155.

Goddard, L. and Dilley, M. 2005. El Niño: Catastrophe or Opportunity. *J. Climate* **18**, 651–665.

Gu, D. and Philander, S. G. H. 1995. Secular changes of annual and interannual variability in the tropics during the past century. *J. Climate* **8**, 864–876.

Guilyiardi, E. 2006. El Niño mean state-seasonal cycle interactions in a multimodel ensemble. *Clim. Dyn.*, **26**, 329–348.

Harshvardhan, R., Davies, R., Randall, D. A. and Corsetti, T. G. 1987. A fast radiation parameterization for atmospheric circulation models. *J. Geophys. Res.* **92**(D1), 1009–1016.

Holtslag, A. A. M. and Moeng, C.-H. 1991. Eddy diffusivity and countergradient transport in the convective atmospheric boundary layer. *J. Atmos. Sci.* **48**, 1690–1698.

Hong, S. Y. and Pan, H. L. 1996. Nonlocal boundary layer vertical diffusion in a medium range forecast model. *Mon. Wea. Rev.* **124**, 2322–2339.

Horel, J. D. and Wallace, J. M. 1981. Planetary-scale atmospheric phenomena associated with the Southern Oscillation. *Mon. Wea. Rev.* **109**, 813–829.

Hoskins, B. J. and Karoly, D. J. 1981. The Steady Linear Response of a Spherical Atmosphere to Thermal and Orographic Forcing. *J. Atmos. Sci.* **38** 1179–1196.

Huang, B. 2004. Remotely forced variability in the tropical Atlantic Ocean. *Clim. Dyn.* **23**, 133–152, doi:10.1007/s00382-004-0043-8.

Ineson, S. and Davey, M. K. 1997. Interannual climate simulation and predictability in a coupled TOGA GCM. *Mon. Wea. Rev.* **125**, 721–741.

International GEWEX Project Office 2002. *The Second Global Soil Wetness Project Science and Implementation Plan.* IGPO Publication Series No. 37, 69 pp.

Jin, F.-F. 1997. An equatorial recharge paradigm for ENSO. Part I: conceptual model. *J. Atmos. Sci.* **54**, 811–829.

Joseph, R. and Nigam, S. 2006. ENSO evolution and teleconnections in IPCC's 20th century climate simulations: realistic representation? *J. Climate* **19**, 4360–4377.

Kalnay, E., Kanamitsu, M., Kistler, R., Collins, W., Deaven, D. and co-authors. 1996. The NCEP/NCAR 40-year reanalysis project. *Bull. Amer. Soc.* **77**, 437–471.

Kiehl, J. T., Hack, J. J., Bonan, G., Boville, B. A., Williamson, D. L. and co-authors. 1998. The National Center for Atmospheric Research Community Climate Model: CCM3. *J. Climate* **11**, 1131–1149.

Kirtman, B. P. 1997. Oceanic rossby wave dyanmics and the ENSO period in a coupled model. *J. Climate* **10**, 1690–1704.

Kirtman, B. P. 2003. The COLA anomaly coupled model: ensemble ENSO prediction. *Mon. Wea. Rev.* **131**, 2324–2341.

Kirtman, B. P. and Shukla, J. 2002. Interactive coupled ensemble: a new coupling strategy for GCMs. *Geophys. Res. Lett.* **29**, 1029–1032.

Kirtman, B. P., Fan, Y. and Schneider, E. K. 2002. The COLA global coupled and anomaly coupled ocean atmosphere GCM. *J. Climate* **15**, 2301–2320.

Krishnamurthy, V. and Kirtman, B. P. 2003. Variability of the Indian Ocean: relation to monsoon and ENSO. *Quart. J. Roy. Meteor. Soc.* **129**, 1623–1646.

Kumar, A. and Hoerling, M. P. 1998. Annual cycle of Pacific-North American seasonal predictability associated with different phases of ENSO. *J. Climate* **11**, 3295–3308.

Large, W. G., McWilliams, J. C. and Doney, S. C. 1994. Oceanic vertical mixing: a review and a model with a nonlocal boundary layer parameterization. *Rev. of Geophys.* **32**, 363–403.

Latif, M., Sperber, K., Arblaster, J., Braconnot, P., Chen, D. and co-authors. 2001. ENSIP: The El Niño simulation intercomparison project. *Clim. Dyn.* **18**, 255–272.

Lau, N.-C. and Nath, M. J. 1996. The Role of the "Atmospheric Bridge" in Linking Tropical Pacific ENSO Events to Extratropical SST Anomalies. *J. Climate* **9**, 2036–2057.

Levitus, S. 1982. *Climatological World Atlas of the Ocean.* US Govt. printing office. 173 pp.

Marx, L. 2002. New calculation of saturation specific humidity and saturation vapor pressure in the COLA atmospheric general circulation model. Available from ftp://grads.iges.org/pub/ctr/ctr_130_text.pdf.

Mechoso, C. R., Robertson, A. W., Barth, N., Davey, M. K., Delecluse, P. and co-authors. 1995. The seasonal cycle over the torpical Pacific in coupled Ocean-Atmosphere general circulation models. *Mon. Wea. Rev.* **123**, 2825–2838.

Meehl, G. A. and Arblaster, J. M. 1998. The Asian-Australian Monsoon and El Niño Oscillation in the NCAR Climate System Model. *J. Climate* **11**, 1356–1385.

Mellor, G. L. and Yamada, T. 1982. Development of a turbulence closure model for geophysical fluid processes. *Rev. Geophys. Space Phys.* **20**, 851–875.

Moorthi, S. and Suarez, M. J. 1992. Relaxed Arakawa-Schubert. A parameterization of Moist Convection for General Circulation Models. *Mon. Wea. Rev.* **120**, 978–1002.

Meinen, C. S. and McPhaden, M. J. 2000. Observations of warm water volume changes in the equatorial Pacific and their relationship to El Niño and La Niña. *J. Climate* **13**, 3551–3559.

Neelin, J. D., Latif, M., Allaart, M. A. F., Cane, M. A., Cubasch, U. and co-authors. 1992. Tropical air-sea interaction in general circulation models. *Clim. Dyn.* **7**, 73–104.

Nigam, S., Chung, C. and DeWeaver, E. 2000. ENSO diabatic heating in ECMWF and NCEP-NCAR reanalyses and NCAR CCM3 simulation. *J. Climate* **13**, 3152–3171.

Nigam, S. and Chung, C. 2000. ENSO surface winds in CCM3 simulations: diagnosis of errors. *J. Climate* **13**, 3172–3186.

Pacanowski, R. C. and Griffies, S. M. 1998. MOM3.0 manual, NOAA/Geophysical Fluid Dynamics Laboratory, Princeton, New Jersey, USA 08542.

Philander, S. G. H. 1983. El Niño-Southern Oscillation phenomena. *Nature* **302**, 295–301.

Philander, S. G. H. 1990. *El Niño, La Niña and the Southern Oscillation.* Academic Press, San Diego, USA, pp. 293.

Philander, S. G. H. 2001. *El Niño* Southern Oscillation (ENSO) Models. In: *Encyclopedia of Ocean Sciences* (eds J. H. Steele, S. A. Thorpe, and K. K. Thurekian), Academic Press, London.

Rao, K. A. and Sperber, K. 2006. ENSO simulation in coupled ocean-atmosphere models: are the current models better? *Clim. Dyn.* **27**, 1–15, doi:10.1007/s00382-006-0119-7.

Rasmusson, E. M. and Carpenter, T. H. 1982. Variations in Tropical Sea Surface Temperature and Surface Wind Fields Associated with the Southern Oscillation/ El Niño. *Mon. Wea. Rev.* **110**, 354–384.

Rayner, N. A., Parker, D. E., Horton, E. B., Folland, C. K., Alexander, L. V. and co-authors. 2002. Global analyses of sea surface temperature, sea ice and night marine air temperature since the late nineteenth century. *J. Geophys. Res.* **108**, doi:10.1029/2002JD002670.

Redi, M. H. 1982. Oceanic isopchynal mixing by coordinate rotation. *J. Phys. Oceanography* **11**, 1443–1451.

Ropelewski, C. F. and Halpert, M. S. 1987. Global and Regional scale precipitation patterns associated with the El Niño/Southern Oscillation. *Mon. Wea. Rev.* **115**, 1606–1626.

Rosati, A., Gudgel, R. and Miyakoda, K. 1997. The impact of ocean initial conditions on ENSO forecasting with a coupled model. *Mon. Wea. Rev.* **125**, 754–772.

Schneider, E. K. 2002. Understanding differences between the Equatorial Pacific as simulated by two coupled GCMs. *J. Climate* **15**, 449–469.

Smagorinsky, J. 1963. General circulation experiments with the primitive equations: I. The basic experiment. *Mon. Wea. Rev.* **91**, 99–164.

Straus, D. and Shukla, J. 2000. Distinguishing between the SST-forced variability and internal variability in mid-latitudes: analysis of observations and GCM simulations. *Quart. J. Roy. Meteor. Soc.* **126**, 2323–2350.

Suarez, M. J. and Schopf, P. S. 1988. A delayed action oscillator for ENSO. *J. Atmos. Sci.* **45**, 549–566.

Tiedtke, M. 1984. The effect of penetrative cumulus convection on the large-scale flow in a general circulation model. *Beitr. Phys. Atmos.* **57**, 216–239.

Timmermann, A., 1999. Detecting the nonstationary response of ENSO to greenhouse warming. *J. Atm. Sci.* **56**, 2313–2325.

Trenberth, K. E., Branstator, G. W., Karoly, D., Kumar, A., Lau, N.-C., and co-authors. 1998. Progress during TOGA in understanding and modelling global teleconnections associated with tropical sea surface temperatures. *J. Geophys. Res.* **103**, 14 291–12 324.

Troen, I. and Mahrt, L. 1986. A simple model of the atmospheric boundary layer. Sensitivity to surface evaporation. *Bound Layer Meteor.* **37**, 129–148.

Tziperman, E., Zebiak, S. E. and Cane, M. A. 1997. Mechanisms of seasonal-ENSO interactions. *J. Atmos. Sci.* **54**, 61–71.

van Oldenborgh, G. J., Philip, S. and Collins, M. 2005. El Niño in a changing climate: a multimodel study. *Ocean Sci.* **1**, 81–95.

Wang, B. 1995. Interdecadal changes in El Niño onset in the last four decades. *J. Climate* **8**, 267–285.

Wu, R., Kirtman, B. P. and Pegion, K. 2006. Local Air-sea relationship in observations and model simulations. *J. Climate*, **19,** 4914–4932.

Xie, P. and Arkin, P. 1996. Analysis of global monthly precipitation using guage observations, satellite estimates and numerical model predictions. *J. Climate* **9**, 840–858.

Xue, Y.-K., Sellers, P. J., Kinter, J. L. and Shukla, J. 1991. A simplified biosphere model for global climate studies. *J. Climate* **4**, 345–364.

Xue, Y.-K., Zeng, F. J. and Schlosser, C. A. 1996. SSiB and its sensitivity to soil properties. A case study using HAPEX-Mobilhy data. *Global Planetary Change* **13**, 183–194.

Yang, X. Q. and Anderson, J. L. 2000. Correction of systematic errors in coupled GCM forecasts. *J. Climate* **13**, 2072–2085.

Zelle, H., Appeldoorn, G., Burgers, G. and van Oldenborgh, G. J. 2004. The relationship between sea surface temperature and thermocline depth in the Eastern Equatorial Pacific. *J. Phys. Oceanography* **34**, 643–655.